Impact of Cyclic Bending on Coronary Hemodynamics

Jiaqiu Wang[1,2*], Runxin Fang[3], Hao Wu[3], Yuqiao Xiang[1,2], Jessica Benitez Mendieta[1,2], Phani Kumari Paritala[1,2], Zhenya Fan[1], Haveena Anbananthan[1,2], Jorge Alberto Amaya Catano[1,2], Owen Christopher Raffel[4,5] and Zhiyong Li[1,2,3*]

[1*]School of Mechanical, Medical and Process Engineering, Queensland University of Technology, Brisbane, 4000, QLD, Australia.

[2]Centre for Biomedical Technologies, Queensland University of Technology, Brisbane, 4000, QLD, Australia.

[3]School of Biological Science & Medical Engineering, Southeast University, Nanjing, 210096, Jiangsu, China.

[4]Department of Cardiology, The Prince Charles Hospital, Chermside, 4032, QLD, Australia.

[5]School of Medicine, University of Queensland, St Lucia, 4072, QLD, Australia.

*Corresponding author(s). E-mail(s): jiaqiu.wang@hotmail.com; zylicam@gmail.com;

Abstract

It remains unknown that the degree of bias in computational fluid dynamics (CFD) results without considering coronary cyclic bending. This study aims to investigate the influence of different rates of coronary cyclic bending on coronary hemodynamics. To model coronary bending, a multi-ring-controlled fluid-structural interaction (FSI) model was designed. A coronary artery was simulated with various cyclic bending rates (0.5s, 0.75s and 1s, corresponding to heart rates of 120bpm, 80bpm and 60bpm) and compared against a stable model. The simulated results show that the hemodynamic parameters of vortex Q-criterion, temporal wall shear stress (WSS), time-averaged WSS (TaWSS) and oscillatory shear index (OSI) were sensitive to the changes in cyclic rate. A higher heart rate resulted in higher magnitude and larger variance in the hemodynamic parameters. Whereas the values and distributions of flow velocity and relative residence time (RRT) did not show significant differences between different bending periods. This study suggests that a stable coronary model is not sufficient to represent the hemodynamics in a bending coronary artery. Different heart rate conditions were found to have significant impact on the hemodynamic parameters. Thus, the cyclic bending should be considered to mimic the realistic hemodynamics in future patient-specific coronary hemodynamics studies.

Keywords: Coronary cyclic bending, Hemodynamics, Fluid-structure interaction

1 Introduction

Computational fluid dynamics (CFD) has been widely used to simulate coronary hemodynamics. Unlike other blood vessels, coronary arteries adhere to the myocardium, which induces complicated movement and deformation following the cardiac cycle. A CFD model, with a rigid geometric fluid domain, cannot mimic the superposition of changes in position, curvature, and torsion along the coronary artery axis and the variations on the lumen cross-section (Freidoonimehr et al., 2022). The degree of bias in hemodynamic results introduced by omitting the vessel wall elasticity and deformation remains a controversial issue. It has been reported that when replacing the rigid wall with the elastic wall, the effect of wall compliance on the temporal wall shear stress (WSS) was more significant than that on the time-averaged WSS (TaWSS) and oscillatory shear index (OSI) (Torii et al., 2009)(Eslami et al., 2020). When considering the dynamic movement of the coronary vessel, applying a flexible fluid domain in CFD becomes complicated, due to the complexity of defining the coronary motion and setting up the dynamic mesh (Zeng and Ethier, 2003). A practical technology to describe the coronary motion is to attach the coronary surface to a sphere with curvature variation. With this model, the effects of curvature variation were found different in the systolic and diastolic phases (Prosi et al., 2004). Some other key findings of the influence of coronary motion on the hemodynamics include that temporal WSS was more significantly impacted compared to the TaWSS (Zeng et al., 2003)(Torii et al., 2009)(Hasan et al., 2013). And the cyclic bending has a more modest effect on the hemodynamic parameters compared to the structural stress and strain (Tang et al., 2009)(Tang et al., 2009)(Fan et al., 2014).

Compared to the pure CFD model with dynamic mesh, a promising computational model to mimic the temporal variation of coronary would be the fluid-structure interaction (FSI) model, which used the structural domain 'pass' the deformation to the fluid domain, avoiding the complexity of controlling dynamics mesh. However, currently most FSI-based coronary computational models only focus on wall compliance and do not consider a realistic coronary bending. And a more feasible approach to precisely mimic the coronary cyclic bending is urged to further understand the influence of cyclic bending on the coronary hemodynamics.

This study aims to gain a comprehensive understanding of the influence of coronary cyclic bending on hemodynamic factors. In order to mimic the coronary artery movement during the cardiac cycle, a multi-ring-controlled FSI model was designed. The coronary models under various cyclic bending rates (0.5s, 0.75s and 1s, corresponding to heart rates of 120bpm, 80bpm and 60bpm) were simulated and compared with a stable model.

2 Methods

2.1 Coronary Geometric Model

A patient-specific (male, age 54) coronary lumen was reconstructed by extruding the circular intersecting surface (3 mm diameter) through a digital subtraction angiography (DSA)-generated right coronary artery (RCA) centreline. The reconstructed model started after the branch of the acute marginal artery and ended before the branch of the right descending artery, covering the mid to distal range of RCA. The arterial wall was inflated with a uniform thickness of 0.75 mm. Straight extensions were added to both inlet and outlet (Figure 1), to avoid the boundary effects from fluid and extreme distortion at the coronary inlet and outlet.

2.2 Moving Control Rings Module

In order to facilitate the coronary cyclic movement of the reconstructed coronary model, a control-rings module was designed to transfer the displacement profiles onto the arterial wall exteriorly, and subsequently drive the lumen (flow domain) in motion. This module consisted of two fixed rings, which were placed at the two end surfaces of the coronary and 6 moving controllers in between. The movement profiles at each control point were measured from the patient's DSA imaging sequence in one cardiac cycle. To simplify the movement profile, a section of the coronary centreline with endpoints' straight-line distance of 70 mm was cropped. Then the centreline was translated to Cartesian coordinate system by laying the two endpoints onto x-axis. The centroids of controller rings were evenly distributed in the x-direction with a gap of 10 mm. Using these centroids, the rings were defined and were threaded by the coronary model, their circular sectional plane was locally perpendicular to the coronary centreline. A small gap (0.2 mm) was left between the rings and the arterial wall surface. The rings were given movement profiles in y-direction, constrained in x and z directions, and were free to rotate. This setting allowed for a small free relative shift at the contact region, avoiding large spike deformity (Figure 1).

The movement profiles were measured using the displacement at the centroids (only for the 6 moving rings) in the y-direction at different time-points during a cardiac cycle. An in-house developed MATLAB (R2020b, MathWorks,Natick, MA, US) module was used to calculate the displacement and interpolate the movement profiles.

2.3 Computational Model

The FSI simulation was performed on the ANSYS Workbench platform (version 2020R2, ANSYS, Canonsburg, PA, USA). The basic setup of FSI model was following our previous study (Wang et al., 2020). The blood flow through the coronary artery was assumed as laminar incompressible, homogeneous and Newtonian. The viscosity and density were set to $0.00345 Pa \cdot s$,$1050 kg/m^3$, respectively. No-slip boundary was applied to the fluid domain. The mesh movement of fluid dmaoin was controlled by the System Coupling component in ANSYS Workbench, which passed the displacement data from transient structural to Fluent CFD.

The profiles of the coronary velocity and pressure were adopted from a typical RCA flow profile (Broyd et al., 2016). The fluid flow profiles and the coronary movement profiles were mapped into the systolic and diastolic phases. Same as the coronary movement profiles, the cycle periods of flow profiles were scaled to the same cycle periodic times, i.e. 1s, 0.75s and 0.5s (corresponding to heart rates of 60bpm, 80bpm and 120bpm). In the FSI model, the coronary movement profiles and fluid flow profiles with same cyclic period were coupled to simulate the coronary bending under different heart rate.

Considering that the initial status of the coronary model was one of its extreme morphologies (for example, at the highest-y (contraction) or the lowest-y (stretch)), the mono-directional deformation of the coronary in one cardiac cycle may be too large to remove high distortion. To tackle this issue, a medium position was selected as the initial status (a state at time-point of 0). This design was to moderate the distortion and allow the coronary geometry to move bi-directionally from its initial position. Hence, at time 0, the coronary was at a medium position. The time-point 0 to 0.2s was a linear progression period whereby the coronary moved from a medium position to its highest-y (contraction) position. This time-point of 0.2s was set as the initial reference for the entire cardiac cycle. The periodic profiles used in this computational model are plotted in Figure 1.

From the result of each simulation, the hemodynamic parameters, i.e. temporal wall shear stress (WSS), time-averaged WSS (TaWSS), oscillatory shear index (OSI), Relative Residence Time (RRT), velocity and vortex Q-criterion were post-processed in MATLAB and Tecplot EX 360 (2020R2, Tecplot Inc. Bellevue, WA, USA).

In order to intuitively present the influence of cyclic bending, a stable coronary model was conducted to compare against the cyclic bending models. The stable model simulations contained 12 discrete coronary morphologies at different phase in the cardiac cycle using the same boundary conditions as those of the cyclic bending models at the corresponding time phase. Please note unlike the common models which applied varied flow profiles on a stable geometry, the discrete stable model in this study was fully discrete in both geometry and hemodynamics. Therefore, no time-averaged parameters could be provided from the discrete stable model results.

3 Results

3.1 Flow Velocity and Vorticity

From the computational results with three periodic models (0.5s, 0.75s and 1s) and the stable model, the flow velocity magnitude at mid-longitudinal plane at three transient periodic phases were plotted in Figure 2. The velocity range of these four models were similar at the time point with high-velocity inlet (i.e. the second row in Figure 2). The maximum magnitude of velocity presented downtrend following the bending frequency decreasing. In the 0.5s period model the max velocity reached 0.75 m/s, both 0.75s and 1.0s period model had a max velocity of 0.70 m/s, and the stable model had the maximum velocity of 0.67 m/s. At other time points when the inlet velocity profile was low, the four models showed a small and negligible gap in the value range of velocity between each model.

To further evaluate the vorticity, the vortex Q-criterion was used to describe the potential occurrence of vorticity in the blood vessel (Figure 3). The positive Q-criterion tended to appear on the convex side, and inversely, negatives laid on the concave side. Besides, near the buckling location (i.e. the coronary had a larger curvature than surroundings, for example, the locations near #1 and #4 controller rings in Figure 1), the Q-criterion was normally in a high positive value range, meaning the possible existence of vorticity. The span of Q-criterion value followed the trend of velocity waveform. A wider range of Q-criterion was found when velocity magnitude was higher. The results showed that a shorter period resulted in a wider Q-criterion range, which increased the absolute magnitude of both negative and positive Q-values simultaneously. The stable model did not follow this trend. The stable wall had a bit smaller positive Q-values, which indicated less vorticity potential than the flexible wall counterparts. Besides, the stable wall showed a much higher absolute magnitude in the negative Q-values, representing the stronger viscous stress-dominated wall effect.

In order to demonstrate the changes in flow velocity and vortex in one cardiac cycle, the velocity magnitude and the vortex Q-criterion at the centroids of six moving control rings (which are located in the middle centreline of the coronary and distributed evenly in horizontal x-direction, refer to Figure 1) in one periodic cycle were plotted in Figure 4. The velocity pattern at these locations mainly followed the prescribed velocity profile. At the same time point, the velocity magnitude at different locations had small gaps. In the plot of the Q-criterion, positive Q values were found dominant in locations 1, 4 and 6, which were identified as vorticity-dominant area. And the Q values at location 3 and 5 were around zero as a balance of spin and shear. Contrarily the 2nd location consisted of more negative Q values, which was viscous stress dominated location.

3.2 Surface Wall Shear

Similar to the above plot of velocity and Q-criterion, the temporal WSS contours at the three specific time phases were plotted in Figure 5. The shorter period model shows a higher value of WSS than the counterparts with longer periods, especially at the time-point of maximum velocity. At the maximum velocity time-point, the bending model produced a much higher maximum WSS value (over 10 Pa) than the stable model (8.6 Pa), while at the low-velocity time, the difference of max WSS was small. Additionally, the WSS at the concave side (bottom boundary) of the lumen surface was higher than on the convex side (top boundary). In Figure 6, the WSS range on the convex and concave lines during one cycle was presented using a box-plot. The distribution shows that a shorter cycle period brought high magnitude of WSS, at both concave and convex sides. Furthermore, The WSS on the concave side was remarkably higher than on the convex side particularly at time points with high velocity. For example, for the 0.5s period model, the highest WSS on the concave side was 12.0 Pa, alternately, on the convex side was 5.9 Pa.

3.3 Period-averaged Parameters

Three period-averaged WSS-derived hemodynamic parameters, TaWSS, OSI and RRT were exported from the simulation result. From the contours of these parameters (Figure 7), the TaWSS and OSI of the three models were significantly different. The 0.5s period model has more regions with high TaWSS and OSI, the 0.75s period model had less high-value regions and the 1.0s period model had the smallest regions of high TaWSS and OSI. Alternatively, the distribution of RRT was observed to be similar in all models.

The histograms (Figure 8) present the statistical distribution of these period-averaged hemodynamic parameters. From left to right, the period time (0.5s, 0.75s and 1s) increases, corresponding to the heart rate of 120 bpm, 80 bpm and 60 bpm. Overall, TaWSS and OSI were more sensitive to the change of cycle time and RRT was shown to less sensible when the cyclic period varied. A statistics of median, mean, max and standard deviation values (Table 1) explicitly displays the trend of the changes in hemodynamic parameters changing over different periods. The 0.5s period model presented higher TaWSS than the others. The mean value of TaWSS surpassed the 0.75s and 1.0s models by 36.5% and 53.2% respectively. And the maximum value exceeded 0.75s and 1.0s models by 39.9% and 54.3% respectively. The 0.5s model also had a broader range of the values compared to the 0.75s and 0.1s period models. The standard deviation was 35.4% and 52.4% more than that in 0.75s and 1.0s models respectively. Similar for the OSI, taking the 0.5s period model as reference, the mean values from 0.75s and 1.0s periodic model decreased by 68.6% and 77.1%, maximum values decreased by 7.5% and 17.6%, and standard deviations decreased by 59.0% and 65.5%. The median, mean, max and deviation of the RRT were similar for all three models.

4 Discussion

4.1 'Variants' and 'Invariants'

From the simulation results, the vortex Q-criterion, WSS, TaWSS and OSI were found sensitive to changes in the cyclic period which corresponds to the heart rate. The period variance did not have a large impact on flow velocity and RRT. Here the variation of these parameters is discussed.

The results of blood flow velocity in this computational model were driven by the velocity and pressure profiles at boundaries. As the cyclic bending could change the inertia force, the flexible flow domain therefore is also assumed to contribute to the flow acceleration. However, velocity did not show an evident trend with the cycle period changing as hypothesised. The velocity at each location was primarily altered based on the tendency of the inlet profile. Normally the blood flow velocity would be expected to increase with an increasing heart rate. However, due to the lack of measured data, the velocity profiles with different cyclic period used in this study had the same velocity magnitude. This may be a reason for consistency of the velocity results of these four models.

RRT is an indicator of the time of residence the molecules spent around the lumen boundary. It evaluates the surface shear condition incorporating the level of the shear and its oscillatory nature (Himburg et al., 2004). In this coronary model, the flow was treated as mono-directional flow therefore only some relatively high RRT regions were observed at the convex side at areas with low-WSS dominant (Figure 7). In another aorta-based study, high-RRT was observed at the concave side (Soulis et al., 2011). In their model, the high-RRT were found at the concave side and surrounding the branches. The branch area with local vortex normally elevated OSI. Therefore, the high RRT in the aorta was caused by high-OSI. The high-OSI also made the magnitude of RRT from the aforementioned aorta model much higher than that in our models. It is expected that if the branch of the coronary was included in this model, the RRT would then elevate at the branch area and become more dependent on OSI. Hence, it is difficult to predict whether the RRT would be more sensitive to the cycle period changing.

4.2 Why does the heart rate matters?

This study simulated the hemodynamics in coronary under different heart rate. The cycle time (corresponded to heart rate) was proven to have significant influence on key hemodynamic parameters such as WSS and OSI. For example, high heart rate increases the magnitudes of WSS and OSI.

From the conventional rigid-wall CFD model, the difference of thermodynamics under different heart rate may not be revealed. In Figure 9, the period-averaged wall shear derivative parameters were plotted using conventional rigid-wall CFD model with a stable mid-position coronary geometry. The results show very similar value range of each parameter between different periods. Please note that because of the nature of stable CFD model, only one transient geometry could be selected for simulation. But these results still could qualitatively prove that there were significant differences on these parameters between cyclic-bending model and stable CFD model.

Therefore, it is clear that the heart rate should be a non-negligible consideration to refine the computational model. For instance, to evaluate the hemodynamics under the exercise scenario, the normal 1s cycle time (60 bpm) cannot be expected to provide realistic results, as it underestimated the magnitude and distribution of WSS and OSI, and may further cause undervaluation of patient vulnerability. Alternatively, the use of boundary conditions with a 0.5s cycle (120 bpm) will be pertinent.

4.3 Advantage of Ring-control Model

In this paper, we proposed the concept of using a series of independent ring units to flexibly control coronary cyclic bending. The highly non-linear, non-uniform and distorted deformation delivered to the fluid domain is achieved by means of FSI computational model. Depending on the length of interest region, cross-section size of coronary, and the complexity of measured deformation profile, the control-ring parameters such as size and quantity can be flexibly adjusted. A future study will target to further provide a strategy of the setup of control rings. The precision of the movement control can be regulated by adding more rings, using finer ring dimensions, allowing more degrees of freedom, and down-sampling the shift measurement based on the computational demand on different patient-specific coronary models. The displacement profiles of each control-ring could be intuitively measured from the DSA imaging data and directly applied to the computational model.

4.4 Limitations

The hemodynamics in the cyclic-bending coronary is complex. The discussion has stated some limitations for the current model setup and discussed process optimisation options, viz:

4.4.1 geometric model limit

In this study, the single tunnel vessel and mono-directional flow was used. The absence of branch structure meant that most of the hemodynamic parameters were under-estimated. As from empirical consensus, the branch area is likely associated with vorticity with abnormal values of hemodynamic parameters such as WSS, OSI and RRT which is subsequently prone to develop atherosclerosis. Due to the flexibility of using controller rings, our cyclic-bending model can be smoothly translated to the coronary model with the branch.

4.4.2 boundary condition

The boundary condition is an inescapable consideration in computational simulations, especially for patient biomechanical modelling. Most of the data used for boundary conditions cannot be directly and adequately measured from the patient. Another complex aspect of coronary modelling is matching the profiles of cyclic bending and hemodynamics. When applying the bending displacement on each control ring, these rings were perfectly synchronized, which meant every point at the coronary was at the same phase. However, when applying the velocity profile at the inlet, the waveform took some time to travel to each location in the coronary, i.e. the hemodynamic parameters tended to have phase displacement at different locations simultaneously. Therefore, the inlet and outlet profiles must match the bending displacement curves where the phases do not match. This problem does not seem to have a solution yet, because it is hard to know the points in lumen where the pulse phase matches with the bending phase, unless a direct measurement of velocity and pressure can be acquired at a known position. Another solution could be to mimic the entire heart structure and the circular path of the coronary vascular system. This avoids the use of velocity and pressure profile from an arbitrary inlet location.

4.4.3 structural analysis

In this study we did not acquire the structural analysis results from FSI model. It is admitted the lack of structural analytical results did weaken the advantage of using FSI model, though the scope of this study was the coronary hemodynamics exclusively. In the current setup of ring-controlled coronary motion model, some issues may arise in the structural analysis. From the design of the ring-control model, the controller rings can be clearly seen to make contact with the vessel wall. This causes local buckling which impacts the stress and strain results. Mild local buckling resulting from the control ring contacting could also be observed in the fluid domain in this study. The potential solution to this occurrence includes: 1) using a relatively softer material for the controller rings, but this might in turn decrease the controlling precision of displacement; 2) adding a sleeving layer in between the control rings and vessel wall structure; and 3) as ascribed, increasing the number of the control-rings which adds contact surface area and smooths the displacement profile.

The solution of enabling structural analysis in the proposed ring-controlled coronary model is planned to be investigated in future study. A more comprehensive model with both structural and hemodynamic analysis is expected to better depict the coronary bending mechanism.

5 Conclusion

A ring controlled FSI model was designed to mimic the hemodynamics in the coronary with various cyclic bending frequencies. The hemodynamic parameters of vorticity Q-criterion, temporal WSS, TaWSS and OSI were found sensitive to the variation cycle period time (i.e. the change of the heart rate). Whereas no significant change in velocity magnitude and RRT were observed from the simulation results. The variation of heart rate has non-negligible effect on the coronary hemodynamics. The conventional stable model and misapplication of cycle period of boundary conditions may significantly underestimate the important hemodynamics parameters and further influence the precision of diagnosis. Therefore, we suggest that in the coronary computational simulation, the effects of both temporal variations in geometry and hemodynamics should be carefully considered, and the boundary condition profiles should be patient-specific, guaranteeing a realistic result.

Acknowledgements

Computational resources and services used in this work were provided by the HPC and Research Support Group, Queensland University of Technology (QUT), Brisbane, Australia. As the receiver of Roland Bishop Award, Dr. Jiaqiu Wang would like to thank the Bishop family for their generous support of Biomedical Engineering Research.

Funding

This work was partially supported by the National Natural Science Foundation of China (Grant Numbers 12172089, 11972118, 61821002), the Australian Research Council (ARC) (Grant Number DP200103492), and the Early Career Researcher Grant funded by Centre for Biomedical Technologies.

Conflict of Interest

The authors declare that they have no conflict of interest.

Author Contribution

J.W. designed the study, setup the computational work, processed data and wrote the manuscript. R.F. and H.W. prepared the figures 2-8. Y.X. processed the statistics. J.M., H.A., J.C. and P.P. participated on designing the study plan. Z.F. optimised the simulation setup. O.R. provided clinical insight on the results discussion. Z.L. supervised the study. All authors reviewed the final manuscript.

References

Broyd, C., J. Davies, J. Escaned, A. Hughes, and K. Parker. 2016. Wave intensity analysis and its application to the coronary circulation. *Global Cardiology Science and Practice 2015*(5): 64 .

Eslami, P., J. Tran, Z. Jin, J. Karady, R. Sotoodeh, M.T. Lu, U. Hoffmann, and A. Marsden. 2020. Effect of wall elasticity on hemodynamics and wall shear stress in patient-specific simulations in the coronary arteries. *Journal of biomechanical engineering 142*(2) .

Fan, R., D. Tang, C. Yang, J. Zheng, R. Bach, L. Wang, D. Muccigrosso, K. Billiar, J. Zhu, G. Ma, et al. 2014. Human coronary plaque wall thickness correlated positively with flow shear stress and negatively with plaque wall stress: an ivus-based fluid-structure interaction multi-patient study. *Biomedical engineering online 13*(1): 1–14 .

Freidoonimehr, N., R. Chin, A. Zander, and M. Arjomandi. 2022. A review on the effect of temporal geometric variations of the coronary arteries on the wall shear stress and pressure drop. *Journal of Biomechanical Engineering 144*(1) .

Hasan, M., D.A. Rubenstein, and W. Yin. 2013. Effects of cyclic motion on coronary blood flow. *Journal of biomechanical engineering 135*(12) .

Himburg, H.A., D.M. Grzybowski, A.L. Hazel, J.A. LaMack, X.M. Li, and M.H. Friedman. 2004. Spatial comparison between wall shear stress measures and porcine arterial endothelial permeability. *American Journal of Physiology-Heart and Circulatory Physiology 286*(5): H1916–H1922 .

Prosi, M., K. Perktold, Z. Ding, and M.H. Friedman. 2004. Influence of curvature dynamics on pulsatile coronary artery flow in a realistic bifurcation model. *Journal of biomechanics 37*(11): 1767–1775 .

Soulis, J.V., O.P. Lampri, D.K. Fytanidis, and G.D. Giannoglou 2011. Relative residence time and oscillatory shear index of non-newtonian flow models in aorta. In *2011 10th international workshop on biomedical engineering*, pp. 1–4. IEEE.

Tang, D., C. Yang, S. Kobayashi, J. Zheng, P.K. Woodard, Z. Teng, K. Billiar, R. Bach, and D.N. Ku. 2009. 3d mri-based anisotropic fsi models with cyclic bending for human coronary atherosclerotic plaque mechanical analysis. *Journal of Biomechanical Engineering* .

Tang, D., C. Yang, J. Zheng, P.K. Woodard, K. Billiar, Z. Teng, and R. Bach 2009. 3d in vivo ivus-based anisotropic fsi models with cyclic bending for human coronary atherosclerotic plaque mechanical analysis. In *Summer Bioengineering Conference*, Volume 48913, pp. 181–182. American Society of Mechanical Engineers.

Torii, R., J. Keegan, N. Wood, A. Dowsey, A. Hughes, G. Yang, D. Firmin, S. Mcg Thom, and X. Xu. 2009. The effect of dynamic vessel motion on haemodynamic parameters in the right coronary artery: a combined mr and cfd study. *The British journal of radiology 82*(special_issue_1): S24–S32 .

Torii, R., N.B. Wood, N. Hadjiloizou, A.W. Dowsey, A.R. Wright, A.D. Hughes, J. Davies, D.P. Francis, J. Mayet, G.Z. Yang, et al. 2009. Fluid–structure interaction analysis of a patient-specific right coronary artery with physiological velocity and pressure waveforms. *Communications in numerical methods in engineering 25*(5): 565–580 .

Wang, J., P.K. Paritala, J.B. Mendieta, Y. Komori, O.C. Raffel, Y. Gu, and Z. Li. 2020. Optical coherence tomography-based patient-specific coronary artery reconstruction and fluid–structure interaction simulation. *Biomechanics and modeling in mechanobiology 19*(1): 7–20 .

Zeng, D., Z. Ding, M.H. Friedman, and C.R. Ethier. 2003. Effects of cardiac motion on right coronary artery hemodynamics. *Annals of biomedical engineering 31*(4): 420–429 .

Zeng, D. and C. Ethier. 2003. A mesh-updating scheme for hemodynamic simulations in vessels undergoing large deformations. *Journal of engineering mathematics 47*(3): 405–418 .

Table 1 Statistical values of the period-averaged WSS-derived parameters.

Parameter	Period	Median	Mean	Max	SD
TaWSS (Pa)	0.5s	3.986	4.054	11.41	1.277
	0.75s	2.467	2.574	6.860	0.8244
	1.0s	1.809	1.897	5.214	0.608
OSI	0.5s	0.01345	0.02241	0.1475	0.02253
	0.75s	0.003851	0.007036	0.1364	0.009217
	1.0s	0.002433	0.005130	0.1216	0.007778
RRT	0.5s	0.5360	0.5775	2.436	0.2189
	0.75s	0.5495	0.5856	2.441	0.2156
	1.0s	0.5585	0.5931	2.380	0.2154

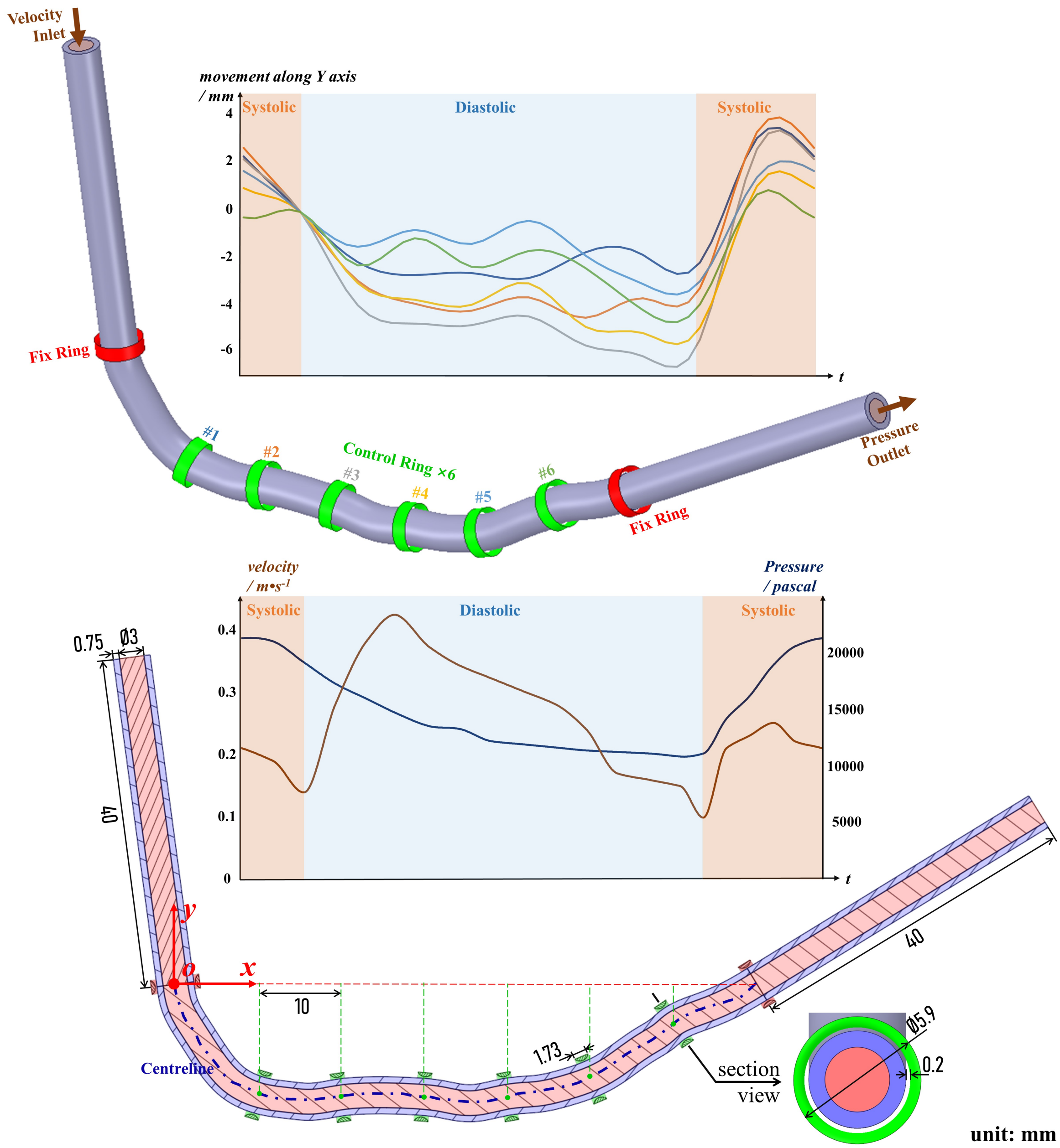

Fig. 1 An overview of the coronary geometric model used in this study. Top: the stereoscopic view of the coronary model, velocity inlet and pressure outlet extensions. Eight rings are equally distributed along the coronary, two of them at boundaries are fixed, while the medium 6 are moving controller, whose periodic shift profiles are plotted in the upright curve chart. Bottom: the lateral cutaway view and the key measurements of the model. Notice that a small gap is left between the rings and the arterial wall surface, which allows small relative shift at the contact region, avoiding large freak deformity. The middle curve chart is the fluid velocity and pressure boundary conditions.

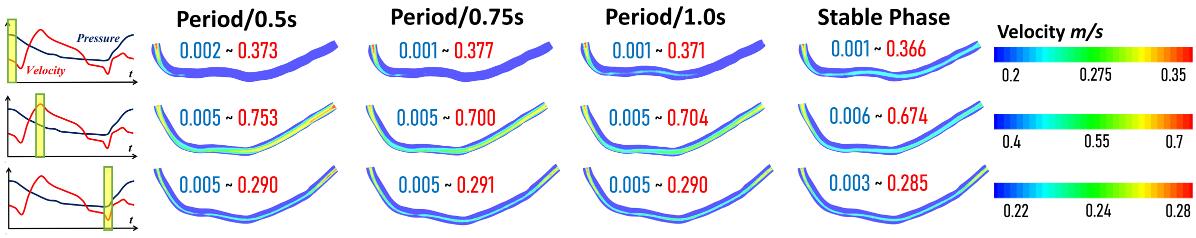

Fig. 2 The velocity contour on the longitudinal section plane at three transient time-points in one periodic cycle. Three transient time-points were selected based on the fluid boundary profiles, from top to bottom rows: the time-phase with the maximum pressure, maximum velocity, and the minimum velocity and pressure. From left to right columns: the results from the computational models with period time of 0.5s (heart rate 120 bpm), 0.75s (80 bpm), 1.0s (60 bpm) and the reference stable model, which was not applied the transient movement and hemodynamic boundary conditions.

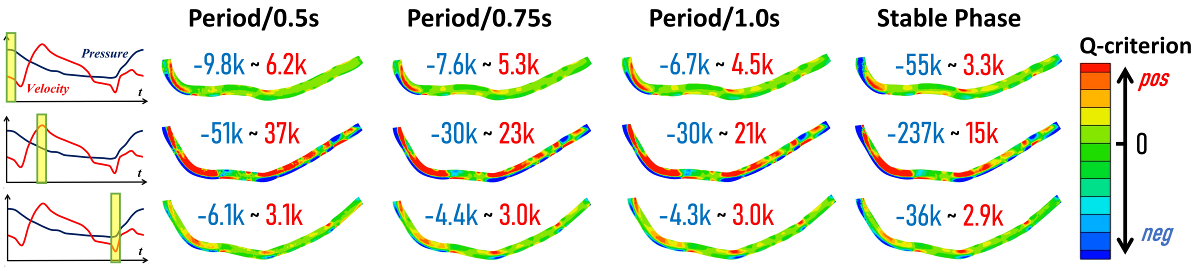

Fig. 3 The contour of vortex Q-criterion on the longitudinal section plane at three transient time-points in one periodic cycle. The value range of Q-criterion for each subplot were labelled. Thereinto, positive values represented vortex dominant area, While the negative values indicated the strain rate or viscous stress dominant area.

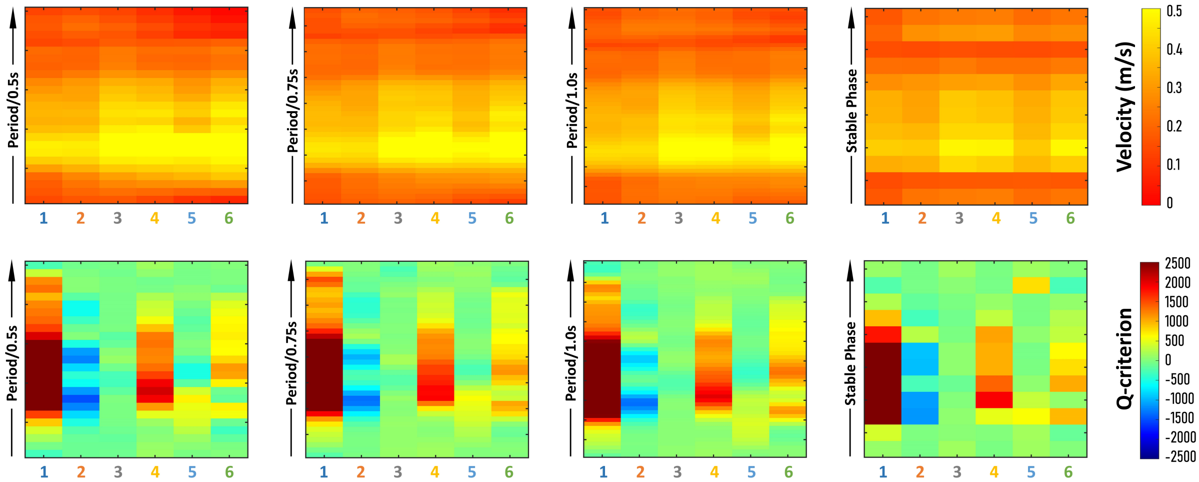

Fig. 4 The velocity (top row) and Q-criterion (bottom row) at the centroids of six moving control rings (the node locations referenced in Figure 1). In each plot, the horizontal axis contains the six centroid points; the vertical axis are the time-phase of one cardiac cycle. Note at each model the number of sample points are not exactly same due to the different periodic time, the data from each models with different period time were normalized and their periodic phase were matched.

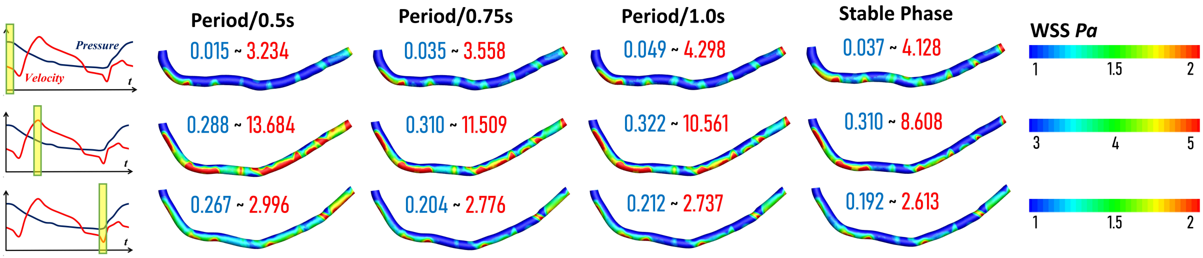

Fig. 5 The contour of lumen surface wall shear stress (WSS) at same three transient time-points in one periodic cycle as Figure 2 and 3. At the time point with high velocity, the WSS pattern showed more significant variance between the four columns (from left to right: 0.5s, 0.75s and 1.0s period time and the reference stable model). A short period time, to wit a high-frequency cycle model brought higher WSS.

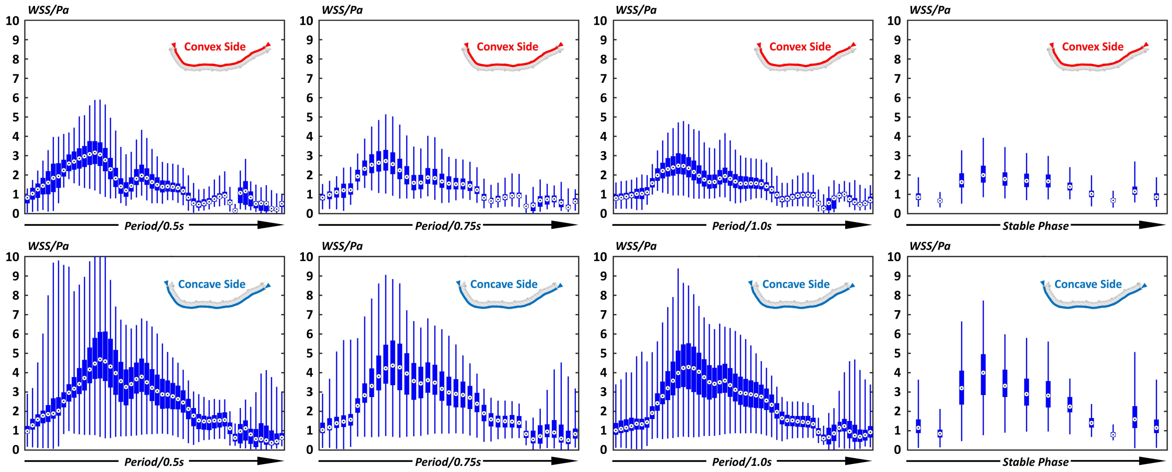

Fig. 6 The histograms of wall shear stress (WSS) on the convex (top) and concave (bottom) lines of coronary lumen surface in the three periodic simulations plus one static simulation. The WSS on the convex side was higher than the concave side. A shorter period (corresponding to high heart rate) resulted in slight higher WSS than the longer period ones. Underestimation of WSS occurred in the stable simulation.

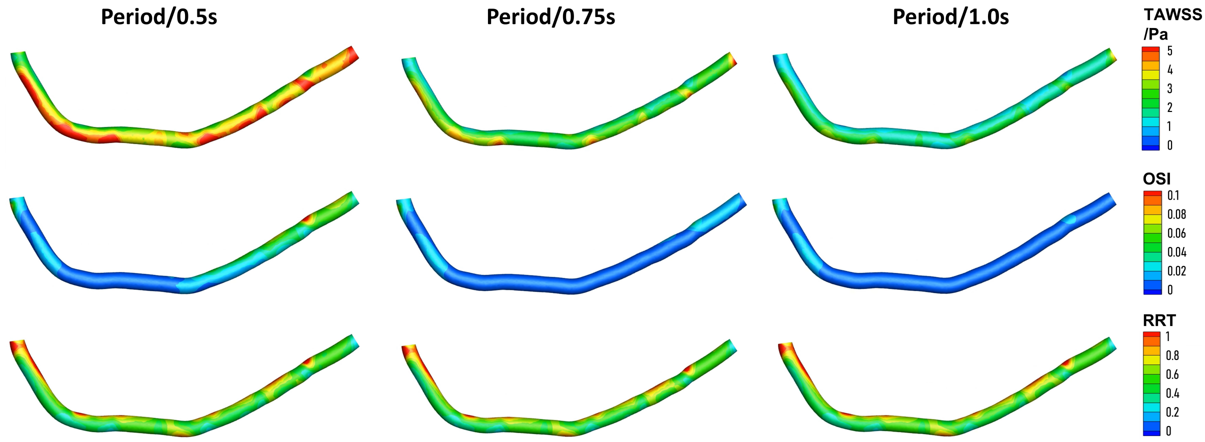

Fig. 7 The contour plot of three period-averaged wall shear derivative parameters on the coronary lumen surface (lateral view). From left to right: three cyclic bending period of 0.5s, 0.75s and 1.0s. From top to bottom: the parameters of time-averaged wall shear stress (TaWSS), oscillatory shear index (OSI) and Relative Residence Time (RRT).

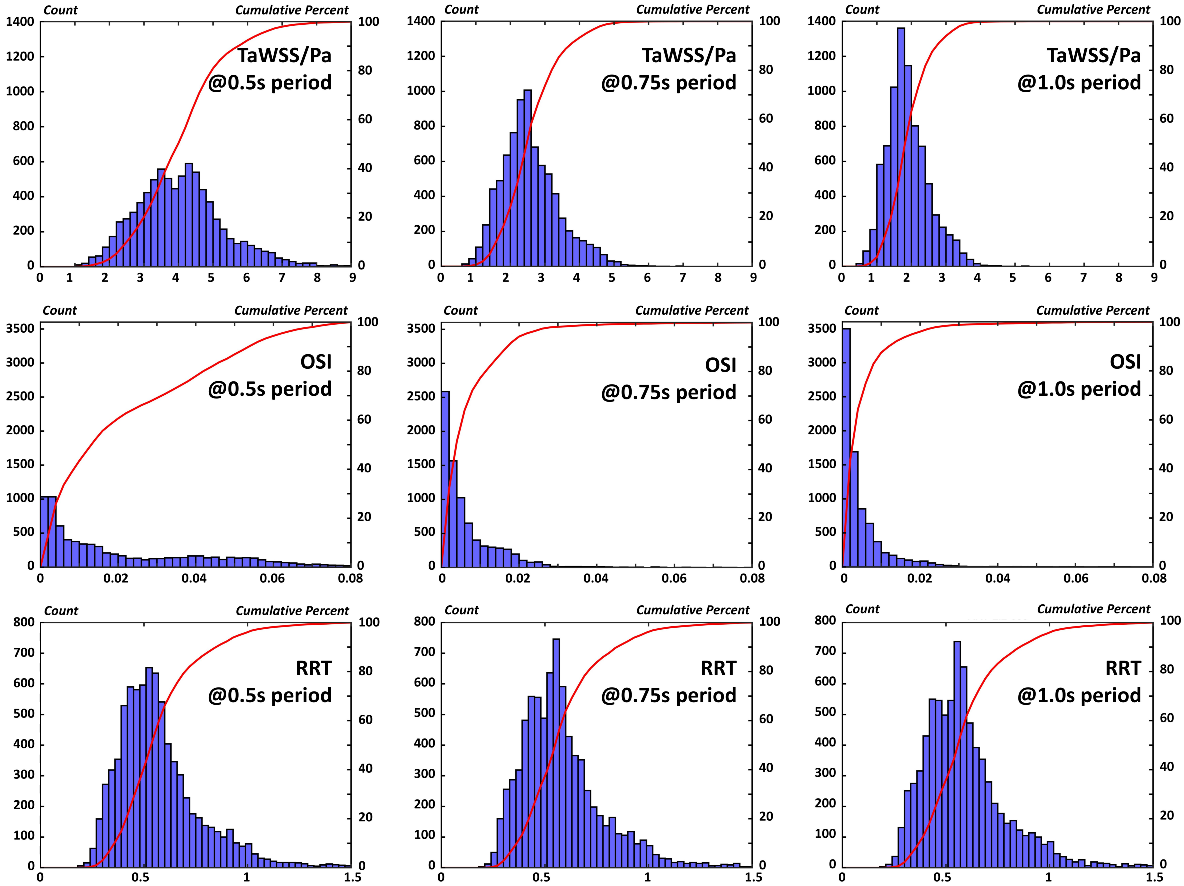

Fig. 8 The histograms of three periodic averaged wall shear derivative parameters on the coronary lumen surface. From left to right: the cyclic bending period of 0.5s, 0.75s and 1.0s. From top to bottom: the parameters of time-averaged wall shear stress (TaWSS), oscillatory shear index (OSI) and Relative Residence Time (RRT). From the histograms, the shorter period (corresponding to high heart rate) resulted in more broad distribution, and higher values of TaWSS and OSI. While no significant distinction was observed in the histograms of RRT from comparing between the three periods.

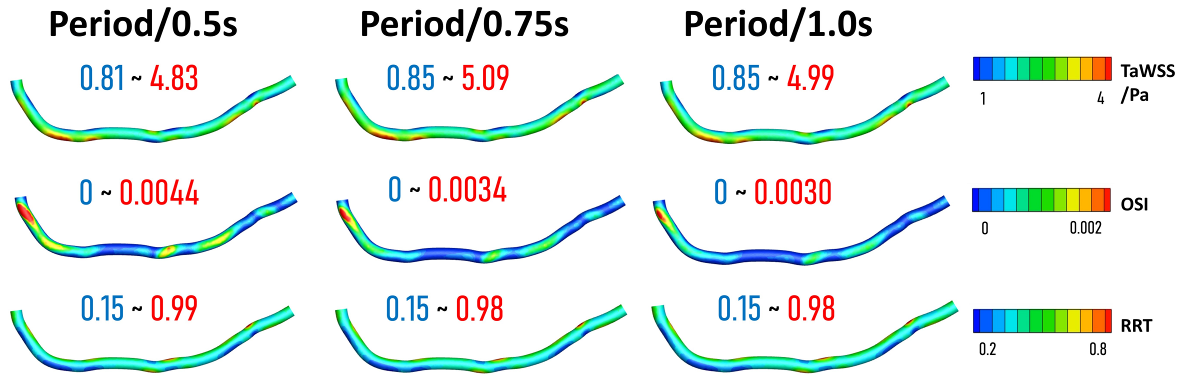

Fig. 9 The contour plot of three period-averaged wall shear derivative parameters on the coronary lumen surface (lateral view). This comparison simulation was performed using conventional rigid-wall CFD model on the initial mid-position of coronary geometry. From left to right: three cyclic bending period of 0.5s, 0.75s and 1.0s. From top to bottom: the parameters of time-averaged wall shear stress (TaWSS), oscillatory shear index (OSI) and Relative Residence Time (RRT).